Paper 145

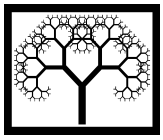

Proceedings of the Eleventh International Conference
on Computational Structures Technology,
B.H.V. Topping, (Editor),
Civil-Comp Press, Stirlingshire, Scotland

The Influence of the Geometric Curvature on the Mechanical Behaviour of the Adhesive Joint

F. Ascione and G. Mancusi
Department of Civil Engineering
University of Salerno, Fisciano (SA), Italy

Abstract

A mechanical model to study the behaviour of a curve adhesive joint is presented. In order to identify the governing parameters of the joint response, the coupling between shear or flexure and the extensional equilibrium problems, the radius of curvature, the energy mobilization corresponding to the most common cohesive interface laws have been introduced. Such model represents a generalization of a previous one introduced by the same authors relative to joint with straight axis. With reference to a concrete beam reinforcement with FRP, a wide numerical investigation has been developed in order to highlight the influence of radius of curvature in terms of absorbed fracture energy as function of the load level.

Keywords: adhesive joints, cohesive fracture, radius of curvature, fibre reinforced polymer, finite element method.

1 Introduction

Until today, in the field of civil engineering, the use of adhesive joints has been principally related to the need of reinforcing pre-existing straight structures made of concrete/masonry by using FRP.
The case of a curve element reinforcement is a problem still to be assessed. The present paper is relative to this framework. In particular, the main scope of the paper is to study the behaviour of curve adhesive joints up to failure and to understand in which way their behaviour is affected by geometrical, mechanical and physical properties of the adherents and adhesive, with particular regard to the geometric curvature.
Recent research works have shown that some parameters play a relevant role, as well as the joint configuration (the thickness of the adhesive layer, the length of the

bonding area, the radius of curvature, etc.) [1-3], the mechanical properties of adherents (bending, axial and shear stiffness) [4] and last but not least the environmental conditions (temperature, moisture etc) [5,6].

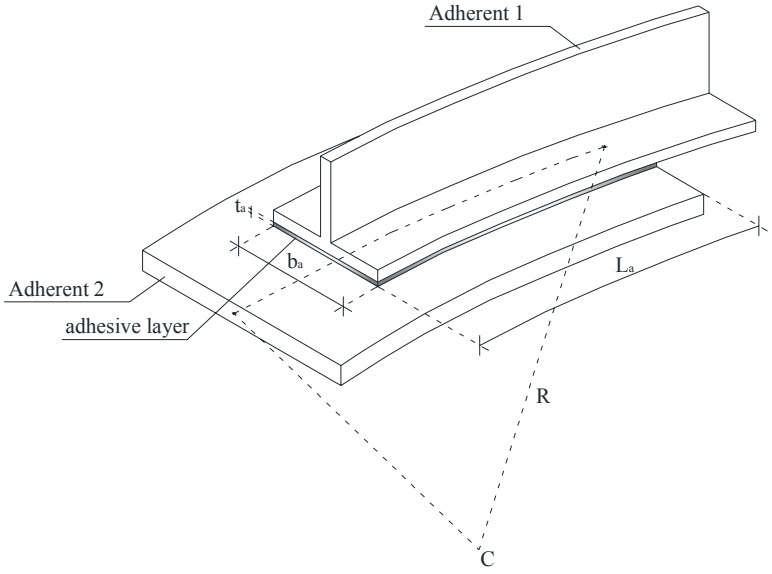

Figure 1: Curve adhesive joint.

The additional presence of shear and flexural stresses, also mobilised by the radius of curvature (Figure 1), even if less relevant in respect to the axial stresses justifies the interest towards more refined approaches which account for mixed mode I/II fracture [7-9].
Within this research field, the paper aims at developing a wide numerical analysis of the behaviour of a generic curve adhesive joint showing the influence of the radius of curvature, relative to adherents and adhesive, in terms of fracture energy absorbed.

2 Mechanical model

In this section the equilibrium problem of a generic curve multi-layered adhesive joint is presented. The adherents are modeled according to the hypotheses of deformability in shear. For what concerns the external load, it is assumed that axial forces (traction/compression) are applied at the end of the joint only.

A schematic representation of such a joint is shown in Figure 2 (single lap joint).

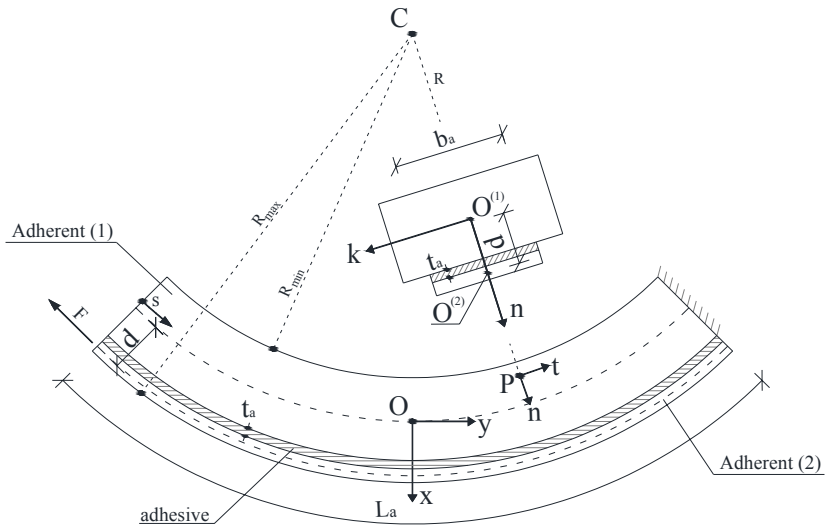

Figure 2: Curve adhesive joint.

For the sake of simplicity in the next Table 1 all symbols introduced in Figure 2 are summarized:

$\{O,x,y,z\}$:	global reference system (Figure 2);
$\{n,t,k\}$:	Frenet unit vectors (Figure 2);
$O^{(1)}$:	centroid of the adherent (1) (Figure 2);
$O^{(2)}$:	centroid of the adherent (2) (Figure 2);
R :	radius of curvature ($R_{min} \le R \le R_{max}$) (Figure 2);
L_a , b_a , t_a :	length, width and thickness of the adhesive layers (Figure 2);
$A^{(1)}$:	cross sectional area of the adherent (1);
$A^{(2)}$:	cross sectional area of the adherent (2);
$I^{(1)}$:	moment of inertia of the adherent (1) (evaluated with respect to the k axis);
$I^{(2)}$:	moment of inertia of the adherent (2) (evaluated in respect to its central axis parallel to k axis);
$E^{(1)}$, $G^{(1)}$:	longitudinal and shear moduli of elasticity of the adherent (1);
$E^{(2)}$, $G^{(2)}$:	longitudinal and shear moduli of elasticity of the adherent (2).

Table 1: Mechanical and geometrical parameters.

The adhesive layer is modelled by continuous distributions of springs, arranged along both the **n** and **t** axes (Figure 3a), able to contrast the relative displacements between the adherents.

The quantities σ and δ (Figure 3b) represent, respectively, the adherents/adhesive interaction per unit surface and the relative transversal displacement, both evaluated along the **n** axis; σ is positive for traction; δ is positive if it corresponds to a separation of the two adherents (i.e. elongation of the spring). Analogously, the quantities τ and s (Figure 3b) represent, respectively, the adherents/adhesive interaction per unit surface and the relative parallel displacement, both evaluated at the interface along the **t** axis; τ is positive if oriented as described in Figure 3b. It is assumed that s has the same sign as τ. Terms δ and s can be related to the generalized displacement components, as indicated in the next sub-section 2.1.

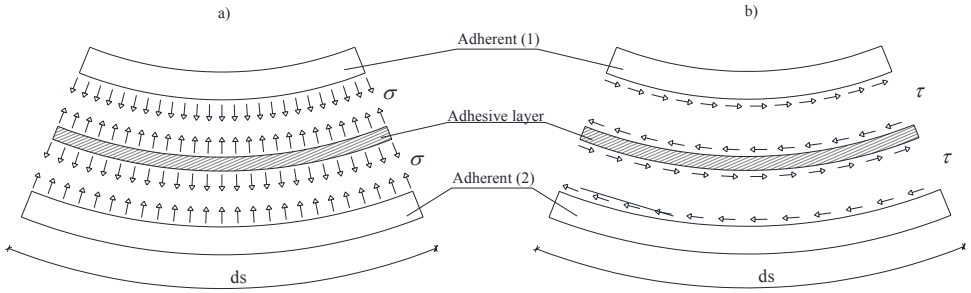

Figure 3: Interfacial interactions: a) normal interactions; b) parallel interactions.

More details about the most common cohesive laws are available in [10]. Generally, for practical purposes, the coupling between the interfacial interactions σ and τ can be simplified by introducing two uncoupled non linear relationships: $\sigma=\sigma(\delta)$ and $\tau=\tau(s)$ (this is equivalent to assume independent springs along **n** and **t** axes) [11]. According to the beam hypotheses here adopted, the only non-trivial strain components within the adherents are the normal and shear ones $\varepsilon_{ss}^{(i)}$ and $\gamma_{ts}^{(i)}$ (i=1,2), which can be related to their corresponding stresses as follows:

$$\sigma_{ss}^{(i)} = E^{(i)}\ \varepsilon_{ss}^{(i)}, \tag{1}$$

$$\tau_{ts}^{(i)} = G^{(i)}\ \gamma_{ts}^{(i)}. \tag{2}$$

2.1 Kinematics and equilibrium

For studying the plane problem depicted in Figure 2 the following displacement field components for the generic *i*-th beam have been adopted:

$$u^{(i)}(n,s) = u_o^{(i)}(s), \tag{3a}$$

$$v^{(i)}(n,s) = v_o^{(i)}(s) + \varphi_o^{(i)}(s)\left(n - n_o^{(i)}\right). \tag{3b}$$

The symbols $u^{(i)}$ and $v^{(i)}$ denote the displacement components of a generic point with reference to the local axes shown in Figure 2 (**n, t**); the symbols $u_o^{(i)}$ and $v_o^{(i)}$ indicate the displacement components of the cross section centroid $O^{(i)}$; the symbol $n_o^{(i)}$ denotes the coordinate of $O^{(i)}$ along the **n** axis; the symbol $\varphi_o^{(i)}$ denotes the flexural rotation of the cross-section and, finally, the symbol s indicates the curvilinear abscissa.
Furthermore, the above introduced quantities $u_o^{(i)}$, $v_o^{(i)}$ and $\varphi_o^{(i)}$, also represent the generalized displacements of the beam model here adopted:

$$\mathbf{u}^{(i)} = \left[u_o^{(i)}, v_o^{(i)}, \varphi_o^{(i)} \right]^T . \tag{4}$$

It is generally easy to express the interfacial interactions, σ and τ, acting at the interface between adherent 1 and adherent 2 (Figure 2), as functions of the kinematical quantities δ and s in the following form:

$$\delta(s) = u_o^{(2)}(s) - u_o^{(1)}(s), \tag{5a}$$

$$s(s) = v_o^{(1)}(s) + \varphi_o^{(1)}(s)\left(n_{interf} - n_o^{(1)}\right) - v_o^{(2)}(s) - \varphi_o^{(2)}(s)\left(n_{interf} - n_o^{(2)}\right). \tag{5b}$$

The symbol n_{interf} denotes the coordinate along the **n** axis of the interface.
With reference to the generic *i-adherent* (i=1,2), the local equilibrium equations which account for the curvature of the joint are the following:

$$\left[\mathbf{\Delta}^T \mathbf{C}^{(i)} \mathbf{\Delta} \right] \mathbf{u}^{(i)} - \mathbf{f}^{(i)} = \mathbf{0}. \tag{6}$$

In equation (6), the operator $\mathbf{\Delta}$, the stiffness matrix $\mathbf{C}^{(i)}$ and the external unit force vector $\mathbf{f}^{(i)}$ assume the following analytical expressions:

$$\mathbf{\Delta}(\cdot) = \begin{bmatrix} -\frac{1}{R} & \frac{d(\cdot)}{ds} & 0 \\ \frac{d(\cdot)}{ds} & \frac{1}{R} & 0 \\ 0 & 0 & \frac{d(\cdot)}{ds} \end{bmatrix}, \quad \mathbf{C}^{(i)} = \begin{bmatrix} E^{(i)}A^{(i)} & 0 & 0 \\ 0 & \frac{G^{(i)}A^{(i)}}{\chi^{(i)}} & 0 \\ 0 & 0 & E^{(i)}I^{(i)} \end{bmatrix}, \tag{7a,b}$$

$$\mathbf{f}^{(i)} = \left[-b_a \cdot \sigma, -b_a \cdot \tau \ , \ b_a \cdot \tau \left(n_o^{(i)} - n_{interf} \right) \right]^T . \tag{7c}$$

In equation (7b) the symbol $\chi^{(i)}$ represent the shear factor of the *i-adherent* and the symbol b_a represents the interface width (Figure 2).

In view of an approximation by means of finite elements, the equilibrium problem of the *i-adherent* (i=1,2) can be expressed in a variational form by using the principle of virtual displacements:

$$\delta \mathrm{L}_{\mathrm{int}}^{(\mathrm{i})} = \delta \mathrm{L}_{\mathrm{interf}}^{(\mathrm{i})} + \delta \mathrm{L}_{\mathrm{ext}}^{(\mathrm{i})} . \tag{8}$$

In equation (8), $\delta \mathrm{L}_{\mathrm{int}}^{(\mathrm{i})}$ is the internal virtual work related to the stresses $\sigma_{\mathrm{ss}}^{(\mathrm{i})}$ and $\tau_{\mathrm{ss}}^{(\mathrm{i})}$; $\delta \mathrm{L}_{\mathrm{interf}}^{(\mathrm{i})}$ is the external virtual work related to the interfacial interactions σ and τ; $\delta \mathrm{L}_{\mathrm{ext}}^{(\mathrm{i})}$ is the virtual work of the external forces. It is important to remark that only external loads applied at the ends of the adherents are taken into account.
The three terms in equation (8) can be represented in an explicit form as indicated below.

$$\delta \mathrm{L}_{\mathrm{int}}^{(\mathrm{i})} = \int_{s_0^{(\mathrm{i})}}^{s_1^{(\mathrm{i})}} ds \left[\int_{\Sigma_\mathrm{i}} \sigma_{\mathrm{ss}}^{(\mathrm{i})} \, \delta \varepsilon_{\mathrm{ss}}^{(\mathrm{i})} \, d\Sigma_\mathrm{i} + \int_{\Sigma_\mathrm{i}} \tau_{\mathrm{ts}}^{(\mathrm{i})} \, \delta \gamma_{\mathrm{ts}}^{(\mathrm{i})} \, d\Sigma_\mathrm{i} \right], \tag{9a}$$

$$\delta \mathrm{L}_{\mathrm{interf}}^{(\mathrm{i})} = \int_{s_0^{(\mathrm{a})}}^{s_1^{(\mathrm{a})}} \mathrm{b_a} \tau \left[-\delta \mathrm{v}_{\mathrm{o}}^{(\mathrm{i})} + \delta \varphi_{\mathrm{o}}^{(\mathrm{i})} \left(\mathrm{n_{i\,interf}} - \mathrm{n}_{\mathrm{o}}^{(\mathrm{i})} \right) \right] ds + \int_{s_0^{(\mathrm{a})}}^{s_1^{(\mathrm{a})}} \mathrm{b_a} \sigma \delta \mathrm{u}_{\mathrm{o}}^{(\mathrm{i})} ds , \tag{9b}$$

$$\delta \mathrm{L}_{\mathrm{ext}}^{(\mathrm{i})} = \left| \mathrm{V}^{(\mathrm{i})} \delta \mathrm{u}_{\mathrm{o}}^{(\mathrm{i})} + \mathrm{N}^{(i)} \delta \mathrm{v}_{\mathrm{o}}^{(\mathrm{i})} + \mathrm{M}^{(\mathrm{i})} \delta \varphi_{\mathrm{o}}^{(\mathrm{i})} \right|_{s_0^{(\mathrm{i})}}^{s_1^{(\mathrm{i})}} . \tag{9c}$$

In the previous equations $s_0^{(\mathrm{i})}$, $s_1^{(\mathrm{i})}$ denote the abscissa of the two ends of the generic *i-adherent*, while $s_0^{(\mathrm{a})}$, $s_1^{(\mathrm{a})}$ refer to the interface; Σ_i denotes the i-th adherent cross-section. Furthermore, in equation (9c) the shear force, $\mathrm{V}^{(i)}$, the axial force, $\mathrm{N}^{(i)}$ and the flexural moment, $\mathrm{M}^{(i)}$, acting on the i-th adherent, represent the classical generalized loads of the beam theory here adopted.
Finally, in equation (9a), the quantities $\delta \varepsilon_{\mathrm{ss}}^{(\mathrm{i})}$ and $\delta \gamma_{\mathrm{ts}}^{(\mathrm{i})}$ have the following analytical expressions:

$$\delta \varepsilon_{\mathrm{ss}}^{(\mathrm{i})} = \delta \mathrm{v}_{\mathrm{o}}^{\prime(\mathrm{i})} (\mathrm{s}) + \delta \varphi_{\mathrm{o}}^{\prime(\mathrm{i})} (\mathrm{s}) \left(\mathrm{n} - \mathrm{n}_{\mathrm{o}}^{(\mathrm{i})} \right), \tag{10a}$$

$$\delta \gamma_{\mathrm{ts}}^{(\mathrm{i})} = \delta \mathrm{u}_{\mathrm{o}}^{\prime(\mathrm{i})} (\mathrm{s}) + \delta \varphi_{\mathrm{o}}^{(\mathrm{i})} (\mathrm{s}) . \tag{10b}$$

In equations (10), the quantities $(\cdot)'$ represent the partial derivative in respect to the curvilinear abscissa. More details about the finite element approximation of the examined equilibrium problem are presented in [11]. The Hermitian interpolant shape functions have been here introduced in order to approximate the unknown generalized displacements within any finite element.

3 Numerical results and discussion

The problem concerning the restoration of pre-existing concrete curved beams by using CFRP laminates is here presented. The numerical experiments have been involved by using the mechanical model before introduced in order to analyse the mechanical response according to a monotone load-path up to failure, highlighting the influence of the radius of curvature, also depending on the sign of the external load (traction or compression).
With this aim, the authors have studied, in particular, the curve joint scheme depicted in Figure 2, assuming the reinforcement glued at the convex side of the curved member and the mechanical and geometrical parameters of the adherents (reinforcement and support) and adhesive as in Table 2 and 3.

	E	**G**	**A (b x h)**	**I**
	[MPa]	**[MPa]**	**[mm^2]**	**[mm^4]**
Adherent 1: Concrete beam	30000	15000	90000 (300 x 300)	6.75E+8
Adherent 2: CFRP Reinforcement	160000	8000	100 (100 x 1)	8.33

Table 2: Mechanical and geometrical properties of adherents.

In Table 2 the symbols *b* and *h*, represent respectively the width and depth of the cross section of the adherent, while the symbols E, G and I assume the meanings introduced in Table 1. The values of E and G relative to adherent 1, are representative of a typical concrete using in civil engineering; while the values of E and G relative to adherent 2 have been adopted by consulting the manufacturer Technical Data Sheet.
The length of the bonded region (Figure 2) has been assumed equal to 400mm. The cohesive bilinear laws adopted to model the interface behaviour are shown in Figure 4: an elastic linear branch is followed by a softening one. These interfacial laws, reported in the most recent literature [12,13], are sufficiently accurate for technical purposes.

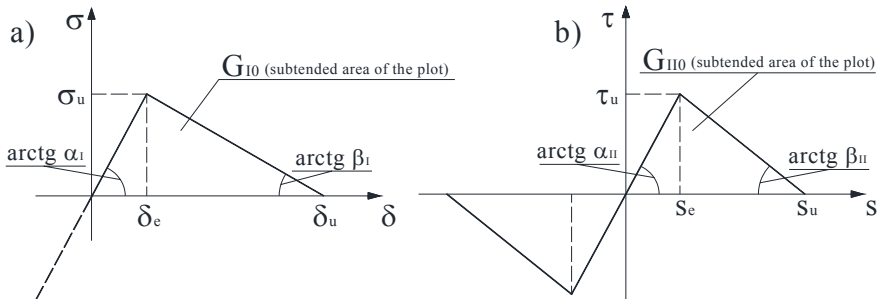

Figure 4: Cohesive laws: a) mode I; b) mode II.

The parameters concerning the Mode II interface law have been established according to Italian Guidelines (CNR DT200/2004) [14]; in relation to the Mode I interface law, due to unavailable data in current literature, a parametric analysis has been developed. In details, the ratio $\alpha = \sigma_u/\tau_u$ has been assumed equal to 0.25 or 2.00 (τ_u fixed) and the elastic and ultimate limits in terms of displacements are the same for both Mode I and Mode II ($\delta_e=s_e$; $\delta_u=s_u$).
Using the symbols of Figure 4, the following values have been considered in the numerical analyses. They are introduced in [14] relative to the epoxy resin commonly used in practice.

s_e	0.015	mm
s_u	0.2	mm
τ_u	4.0	N/mm^2
δ_e	0.015	mm
δ_u	0.2	mm
σ_u	$\alpha\,\tau_u$	N/mm^2

Table 3: Mechanical properties for the interface cohesive model.

3.1 Convergence test and mesh details

The mesh relative to the bonded region (L_a=400mm) is discretized by means of 200 finite elements, as reported in Table 4.

bonded region (length: L_a)	**Number of finite elements**
[mm]	[-]
400.0	200

Table 4: Mesh details.

A convergence test was developed as summarised in Table 5, increasing the number of finite elements used to model the bonded region.

	Number of finite element over the bonding region	**Monitored value**
	0.0mm ÷ 400.0mm	G_{HS}
Test 1	10 (node 1 to 11)	0.837290
Test 2	20 (node 1 to 21)	0.963320
Test 3	50 (node 1 to 51)	0.987970
Test 4	100 (node 1 to 101)	0.992680
Test 5	150 (node 1 to 151)	0.994040
Test 6	200 (node 1 to 201)	0.994680

Table 5: Convergence test.

The convergence assessment is carried out with reference to the value assumed by the quantity $G_{HS} = (G_I/G_{IO}) + (G_{II}/G_{IIO})$, relative to the fracture criterion introduced by Hutchinson and Suo [9] assuming the external force equal to the ultimate numerical one (36.1 kN) evaluated by means of FEM analysis introduced in the previous sections.
In details, referring to the fracture criterion, the numerators of the two fractions represent, respectively, the subtented areas of the two diagrams of Figure 4 for a generic transversal displacement δ and for a generic longitudinal displacement s; while, the denominators of the two fractions represent, respectively, the subtented areas of the aforementioned diagrams for $\delta = \delta_u$ and $s = s_u$.
It appears that a mesh with 200 elements (Test 6) guarantees a sufficient accuracy. The latter has been adopted for the parametric analyses illustrated in the following sections.
For what concerns the radius of curvature, all numerical analyses have been performed neglecting the dependency of R on the position P (Figure 2). This can be justified considering that, when dealing with civil applications, the following condition usually exists: $R_{max} - R_{min} \ll R_{max} + R_{min}$.
Finally, the FEM model above introduced has been formulated as a generalization of a previous one, already validated by the authors in [11] by means of comparisons with other numerical and experimental results available in literature. These comparisons are relative to the case in which the radius of curvature is zero. It is important to remark that no results, relative to the mechanical behaviour of adhesive joint with curve adherents, are available in literature until today.

3.2 Influence of radius of curvature and sign of the external load

In order to highlight the influence of the radius of curvature relative to the sign of the external load, the following values have been considered:

- radius of curvature R=1000 mm and $R \rightarrow \infty$;
- external force F (Figure 2) equal to 15 kN and 30 kN both in traction and in compression. The higher value is close to collapse while the lower one is quite far from the failure;
- $\alpha = \sigma_u/\tau_u = 0.25$ and 2.00.

The results, with reference to the cross-section at s=0 mm (end of the joint, scheme of Figure 2) are summarized in the following tables in terms of :

- actual mode I energy (per unit surface), G_I;
- actual mode II energy (per unit surface), G_{II};
- actual mixed mode I/II interface energy (dimensionless) according to the fracture criterion [9], $G_{HS} \leq 1$.

	Subcase	R	$G_{HS}(s=0)$
	[-]	[mm]	
Traction	1	1000	1.5966E-1
	2	∞	1.5902E-1
	difference	-	-0.4%
Compression	1	1000	1.8632E-1
	2	∞	1.9850E-1
	difference	-	6.13%

Table 6a: (F=15kN; α=0.25).

	Subcase	R	$G_{HS}(s=0)$
	[-]	[mm]	
Traction	1	1000	1.6607E-1
	2	∞	1.6573E-1
	difference	-	-0.2%
Compression	1	1000	1.6744E-1
	2	∞	1.6744E-1
	difference	-	0.00%

Table 6b: (F=15kN; α=2.00).

Observing the results reported in Tables 6, relative to the case of a concrete beam reinforced by means of a CFRP laminate, it is possible to observe the following features:

- if the external load is traction, the effect of the radius of curvature is absent for both cases α=0.25 (about 0.4%) and α=2.00 (about 0.2%);
- if the external load is compression the aforementioned effect is generally beneficial, in the sense of a delay in the energy absorption as the radius of curvature decreases. In details, the beneficial effect is significant in the case α=0.25 (about 6%), while it is substantially absent in the other case: α=2.00.

In order to investigate the possible interaction between the load level and the radius of curvature, the results of Tables 6, have been updated to the case of an external force equal to 30kN, which is representative of the ultimate conditions. The results are reported in Table 7.

	Subcase	R	$G_{HS}(s=0)$
	[-]	[mm]	
Traction	1	1000	6.8290E-1
	2	∞	6.8035E-1
	Max diff.	-	-0.3%
Compression	1	1000	6.8577E-1
	2	∞	6.9597E-1
	Max diff.	-	1.46%

Table 7a: (F=30kN; α=0.25).

	Subcase	R	$G_{HS}(s=0)$
	[-]	[mm]	
Traction	1	1000	6.8443E-1
	2	∞	6.8302E-1
	Max diff.	-	-0.2%
Compression	1	1000	6.8472E-1
	2	∞	6.8370E-1
	Max diff.	-	0.00%

Table 7b: (F=30kN; α=2.00).

By comparing the values of Tables 6 and 7, it is evident that the influence of the radius of curvature becomes less significant as the external load increases independently of its sign (compression or traction). At collapse, no influence has been highlighted in terms of the G_{HS} value.

4 Conclusions

The influence of the radius of curvature on curved adhesive joints, under traction or compression external load, has been studied. With this aim, a mechanical model has been realized, by means of the finite element method, that accounts for the radius of curvature, the shear deformability as well as the coupling effects between axial and shear or flexure behaviour.
Several numerical tests have been conducted. These are relative to the case of the restoration of a pre-existing concrete beam by using FRP system. Schematically the problem is represented by a single lap joints, where the first adherent is made of concrete (support), while the second one is made of FRP (reinforcement). The results have highlighted a different effect of the radius of curvature if the external load is traction (adhesive layer in compression) or compression (adhesive layer in traction). In details, in the first case the aforementioned effect is absent for any load level; in the second one it is observed a beneficial effect, in the sense of a delay in the energy absorption as the radius of curvature decreases. At collapse, no influence has been regarded also for the case relative to external load in compression.

References

[1] A. T. Abdelaziz, R. Boukhili, S. Achiou, S. Gordon and H. Boukehili, “Bonded joints with composite adherends. Part I. Effect of specimen configuration, adhesive thickness, spew fillet and adherend stiffness on fracture”, Int. J Adhes Adhes, 26, 226-236, 2006.

[2] A. T. Abdelaziz, R. Boukhili, S. Achiou and H. Boukehili, “Bonded joints with composite adherends. Part II. Finite element analysis of joggle lap joints”, Int. J Adhes Adhes, 26, 237-248, 2006.

[3] Sato Chiaki, “Stress estimation of joints having adherends with different curvatures bonded with viscoelastic adhesives”, Int. J Adhes Adhes, 31, 315-32, 2001.
[4] M.S. Kafkalidis and M.D. Thouless, “The effects of geometry and material properties on the fracture of single lap-shear joints”, Int. J Solids Struct, 31, 2537-2563, 2002.
[5] K.B. Katnam, J.P. Sargent, A.D. Crocombe, H. Khoramishad and I.A. Ashcroft, “Characterisation of moisture-dependent cohesive zone properties for adhesively bonded joints”, Engineering Fracture Mechanics, 77, 3105-3119, 2010.
[6] L.F.M. da Silva and R. D. Adams, “Joint strength predictions for adhesive joints to be used over a wide temperature range”, Int. J Adhes Adhes, 27, 362-379, 2007.
[7] P.P. Camanho and C. G. Davila, “Mixed-mode decohesion finite elements for the simulation of delamination in composite materials. Report NASA/TM-2002-211737, 2002.
[8] Q.D. Yang and M. D. Thouless, “Mixed-mode fracture analysis of plastically-deforming adhesive joints”, Int. J. of fracture, 110, 175-187, 2001.
[9] J.W. Hutchinson and Z. Suo, “Mixed-mode cracking in layered materials”. Adv Appl Mech, 29, 63-191, 1992.
[10] F. Ascione and G. Mancusi, “Failure criteria for FRP adhesive lap joints: a comparative analysis”, Mech Adv Mater Struc, 17, 157-164, 2010.
[11] F. Ascione and G. Mancusi, “Axial/Bending Coupled Analysis for FRP Adhesive Lap Joints”, Mech Adv Mater Struc, 17, 1-14, 2010.
[12] F. Ascione, “Ultimate behaviour of adhesively bonded FRP lap joints”, Composites Part B, 40, 107-115**,** 2009.
[13] F. Ascione, “Mechanical behavior of FRP adhesive joints: A theoretical model”, Composites Part B, 40, 116-124**,** 2009.
[14] CNR DT 205/2007, “Guide for the Design and Construction of Structures made of FRP Pultruded Elements”, Advisory Committee on Technical Recommendations for Constructions, Italian National Research Council.